

Drop hammer with high-speed thermal imaging

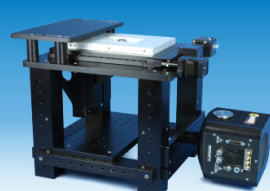

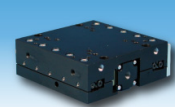
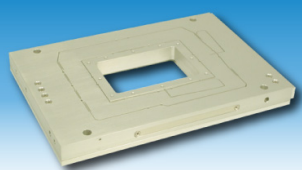

Zhiwei Men, Will P. Bassett, Kenneth S. Suslick, and Dana D. Dlott

Citation: [Review of Scientific Instruments](#) **89**, 115104 (2018); doi: 10.1063/1.5051357

View online: <https://doi.org/10.1063/1.5051357>

View Table of Contents: <http://aip.scitation.org/toc/rsi/89/11>

Published by the [American Institute of Physics](#)



Nanopositioning Systems Micropositioning AFM & SPM Single molecule imaging

Drop hammer with high-speed thermal imaging

Zhiwei Men, Will P. Bassett, Kenneth S. Suslick, and Dana D. Dlott^{a)}

School of Chemical Sciences, University of Illinois at Urbana-Champaign, Urbana, Illinois 61801, USA

(Received 7 August 2018; accepted 18 October 2018; published online 9 November 2018)

The drop hammer test is the easiest way to assess the sensitivity of explosive materials, but drop hammer results for low-velocity impacts have not been able to explain how explosives will react to other kinds of initiating stimuli. In order to do that, we have to understand the fundamental mechanisms of drop hammer initiation and how they differ from other initiation methods. For this reason, there is interest in instrumented drop hammers that help reveal what the drop hammer does at a fundamental level. We have developed a drop hammer that combines two types of mid-wavelength infrared (MWIR) imagers that, when operated simultaneously, can detect both the rapid explosion and slower combustion from impact-initiated polymer-bonded explosives with high time (1 μ s) and space (15 μ m) resolution. Results are presented that show how to vibration isolate the drop hammer to minimize MWIR image shaking during impact and to quantify the noise floor for MWIR temperature determinations via optical pyrometry. Experiments were performed on polymer-encased crystals of RDX ($[\text{CH}_2\text{-NNO}_2]_3$) and HMX ($[\text{CH}_2\text{-NNO}_2]_4$). Our experiments showed that drop-hammer initiated explosions occur in two phases with roughly 100 μ s between explosions. Drop-hammer initiation is compared to an ultrasonic hammer, which initiates explosions by rapid frictional rubbing of the explosive surfaces against the surrounding polymer. The explosion rise time is faster with the drop hammer because the drop hammer inputs energy throughout the explosive volume, whereas the ultrasonic hammer produces localized heating and much more heat at the explosive surface. *Published by AIP Publishing.*
<https://doi.org/10.1063/1.5051357>

I. INTRODUCTION

The drop hammer test^{1–3} is the simplest and easiest way to assess the sensitivity of small amounts of explosives to impact.^{4,5} A hammer weighing a few kg is dropped from a height h at a velocity of a few m/s onto a striker which impacts the test explosive residing on an anvil. The explosive ignites due to localization and concentration of the impact energy at hot spots produced by mechanical failure throughout the explosive.^{2,6} After several trials,⁷ the value of h_{50} , the height that causes 50% of the samples to respond in some obvious way, usually a loud bang or a flash of light, is determined.¹ Many efforts have been made to use measurements of this low-velocity impact h_{50} to predict the results of other explosive initiation methods such as shock initiation, where sensitivity measurements are far more difficult. However h_{50} has not proven to be a reliable predictor of explosive sensitivity under other various insults that might cause initiation.⁴ For this reason, it is important to better understand and evaluate the fundamental mechanisms of drop-hammer initiation of explosives. Moreover, since the mechanism of drop hammer initiation remains poorly understood, it has been difficult to establish deep connections between drop-hammer and other initiation mechanisms.

Drop hammer studies have measured the rate of reaction and extent of reaction using sensors that monitor the pressure wave or gas evolution from the impacted explosives.^{4,8–10} The time lag for getting the wave or gas to the sensor, however, limits the time response of such methods. Drop hammers have

been constructed with transparent anvils so that the impacted explosives can be observed in real time with much faster optical diagnostics. Walley and co-workers reviewed construction principles and test results from such optically accessible drop hammers.¹¹ Using a high-speed video, they observed that impacts which produce a high degree of mechanical deformation in the explosive result in a fast explosion, typically on the order of 100 μ s, followed by slower combustion of material that did not have time to react during the explosion. Williamson and co-workers¹⁰ used an optical drop hammer to study impact initiation of PETN, HMX, and LLM-105. By combining high-speed video using a combination of backlighting and the light from the exploding sample together with mass spectrometry and time-resolved visible emission, they detected hot spot initiation sites and found that at low velocity, LLM-105 underwent a hitherto unobserved low-level reaction. This observation helped explain previous, apparently contradictory sensitivity assessments for LLM-105.¹⁰

Thermal imaging in the infrared (IR) can provide a high speed, nonperturbative method for observing reaction rates and hot spots, but such methods have not been used except in a few cases. Woody^{12,13} developed a drop hammer with an infrared (IR) transmitting window and used high-speed HgCdTe (MCT) detector arrays, either a 4×5 array or a 16×1 array, to image IR emission from shear bands of NaCl crystals.

In the present study, we have developed a drop hammer with high-speed thermal imaging based on mid-wavelength infrared (MWIR) (mid-range infrared 3.7–4.8 μ m) detection and single-color optical pyrometry, which allows us to observe the impacted explosive and measure its temperature evolution in real time. The MWIR detectors are fast enough and

^{a)} Author to whom correspondence should be addressed: dlott@illinois.edu

have a high enough dynamic range, to resolve both the faster explosion and the subsequent slower combustion.¹⁴

The samples used in this study are crystals of explosive materials fully encased in an elastomeric polymer. Encasing the crystals in polymer allows the striker to impact a flat parallel surface, it obviates concerns about frictional heating by abrasives or the surface quality of the striker, and it provides a more realistic environment for the explosion since useful energetic materials are closely packed and often polymer bonded.

No individual thermal imaging detector can, at this time, provide both high spatial resolution images and high time resolution. We have found that this difficulty can be overcome by simultaneously observing the sample with two different kinds of thermal imaging detectors.¹⁴ We previously showed how this combination¹⁴ could be used to observe the dynamics of energetic materials initiated by using an ultrasonic hammer.^{14–16} Here we have incorporated this detector combination into a drop hammer. One detector is a thermal imaging video camera which provides 640×512 MCT detector elements (327 680 pixels) with optics that provide a near-diffraction limited spatial resolution of about $15 \mu\text{m}$.^{14–17} Although this video camera provides excellent high-resolution images, unfortunately its 8.3 ms interframe interval, which is limited by the need to readout 327 680 pixels with a single analog-to-digital converter, is too slow to time resolve the explosion.¹⁴ The second detector was a 32×1 linear array of MCT detector elements. The MCT elements have a nominal rise time of $1 \mu\text{s}$, and each element has its own 4 MHz analog-to-digital converter.¹⁴ Using the 32 high-speed analog-to-digital converters, the overall time response is about $1 \mu\text{s}$ and the linear array produces 4×10^6 line-scan images per second. The linear array captures thermal emission over a smaller field of view than the camera, but it gives the temperature, via single-color pyrometry, at 32 points along a line running through the explosion. The time resolution of the linear array is 33 000 times faster than the video camera. The complementary video camera and linear array thermal imagers produce

both high-resolution images with relatively poor time resolution combined with lower-resolution images with far greater time resolution.¹⁴

In this study, we describe the thermal imaging drop hammer apparatus. It has vibration isolation built into the apparatus, so the image shakes minimally during impact and the hammer does not shake nearby instruments. It has electronic triggering, so the impact can be synchronized with the MWIR imagers. Results will be presented that characterize the thermal explosion from polymer-encased crystals of RDX ($[\text{CH}_2\text{-NNO}_2]_3$) and HMX ($[\text{CH}_2\text{-NNO}_2]_4$). RDX and HMX are widely studied exemplars of high-performance insensitive energetic materials. In addition, we compare the results of our low-velocity impact measurements to results where the same kind of polymer-encased explosive crystals was initiated by friction from high-speed rubbing by using an ultrasonic hammer.^{14–17} This type of comparison is useful to understand how to translate the results of drop-hammer tests to other methods of explosive initiation.

II. INSTRUMENTATION

A. Drop hammer

The drop hammer, shown in Fig. 1 in schematic [Fig. 1(a)] and photographic [Figs. 1(b) and 1(c)] forms, has a weight sled with an adjustable drop height and weight. The drop hammer has an electromagnetic trigger to initiate the sled drop. The falling sled triggers an optical sensor to synchronize the impact with the two fast IR imagers. The drop hammer has vibration isolation to protect surrounding instruments. It is designed to mount the imagers close enough to the sample [Figs. 1(a) and 1(b)] to obtain near diffraction-limited spatial resolution ($15 \mu\text{m}$) in the MWIR. The impact with the striker causes the images to shake, and efforts were made to characterize and minimize image shaking.

The drop hammer is built around a surplus drill press stand. The stand has a cast iron $15'' \times 20''$ base plate with

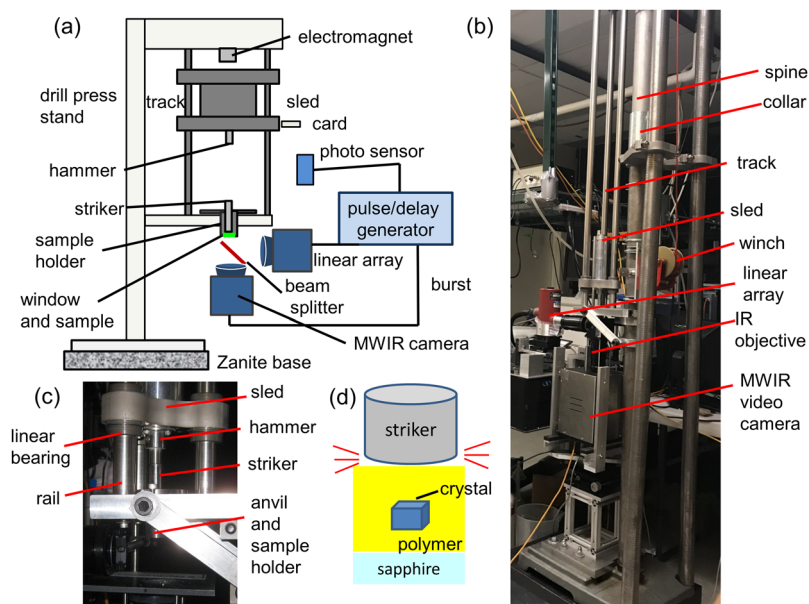


FIG. 1. (a) Schematic of the drop hammer with dual thermal imagers. (b) Photo of the drop hammer. MWIR—mid-wavelength infrared. (c) Close-up of the sled showing the rail, striker, and anvil. (d) Schematic of a striker impacting a polymer-encased crystal.

a 4' long 3" OD cast iron pipe with 1/8" thick walls. This pipe, which formed the "spine" of the drop hammer [Fig. 1(b)], was extended to 95" with a stainless steel (304-SS) pipe with the same OD and wall thickness using a custom-made collar shown in Fig. 1(b). The original drill press version of the drop hammer caused nearby equipment, especially our mode-locked femtosecond lasers, to malfunction when the hammer was dropped, so the drill press was mounted on a 6" thick vibration isolation base plate made from a Zanite Plus polymer-concrete composite (BaseTek LLC) known for its vibration isolation properties. The Zanite Plus base plate had threaded 1/2-13 inserts to bolt it to the drill press and to mount five vibration controlling leveling pads (JW Winco #16NSNS) to the underside.

The weight sled [Figs. 1(b) and 1(c)] has three linear bearings (McMaster-Carr) that ride along a triangular track of three 1" diameter case-hardened 303 stainless steel guide rails 1.0000 ± 0.0005 " diameter with 0.002"/ft straightness (Nordex) [Fig. 1(c)]. The ends of the rods were drilled and tapped to accept 1/4-20 socket-head screws that bolted the rods to the sample holder. The sled carried a stack of 0.5 kg lead weights, and the load could be varied from 0.5 to 4.5 kg.

An end plate mounted on a carrier could be moved along the track to adjust the drop height above the sample from 1" to 40". Assuming a frictionless drop under the acceleration of terrestrial gravity, the impact velocity can range from 0.25 m/s to 10 m/s. The end plate had a 12 V DC, 4.4 W electromagnet with a carrying capacity of 22.6 kg (McMaster-Carr). The top plate of the sled was magnetic iron that could be held by using the electromagnet when it was engaged. The electromagnet is controlled by using an AC to DC electromagnet transformer (McMaster-Carr) with a manual control switch which can reverse current to launch the sled. By varying the height and weight of the sled, the kinetic energy of impact could be varied from 0.015 J to 225 J.

The sled had a card that passed through a photosensor to generate a fast electronic pulse with a 5 μ s rise time, used to trigger a digital delay generator (Stanford Research Systems DG645) which controlled the MWIR cameras. Time $t = 0$ is defined by the trigger pulse, but the trigger pulse was generated when the striker was about 30 mm above the sample. The actual impact occurred at an instant in time that varied with the height of the drop but which was in the 5-10 ms range.

The hammer was a 0.5000 ± 0.0001 " pin gauge made of tool steel with a hardness of C60 on the Rockwell scale (McMaster-Carr). The hammer drives an identical striking pin into the test sample. The striker and hammer pins [Figs. 1(c) and 1(d)] are frequently damaged but easy and inexpensive to replace. The anvils were sapphire windows of 15 mm diameter and 4 mm thickness (Thorlabs). These anvils were transparent in the MWIR region and thick enough to have good survivability to maintain integrity during the thermal imaging measurements.

B. Infrared imagers

For MWIR imaging, we obtained near diffraction-limited resolution of about 15 μ m using a matched pair of 1 \times MWIR microscope objectives having N.A. = 0.22 (Asio

1 \times , Janos Tech, Keene, NH).^{16,17} The video camera (IRE-640M, Sofradir-EC, Inc.) had 15- μ m pitch 640×512 MCT detector elements cooled to 90 K and a cooled prefilter that transmitted light only in the MWIR 3.7–4.8 μ m range. The maximum video rate was 120 Hz (8.33 ms). The camera was used as a single-color pyrometer, as discussed previously.⁷ Single-color pyrometry determines the temperature from the absolute emission intensity integrated over a specific known spectral range, so in order to obtain the temperature, the emissivity must also be known. We used a calibrated blackbody standard (IR-508, Infrared Systems Development) and measured the temperature dependence of RDX crystal emissivity with crystals and binders in a thermostated oven.¹⁶ Due to the close similarity in the chemical structure and optical properties of RDX and HMX, we assumed the measured RDX emissivity for HMX. The linear array detector (TEDAS-3200, Infrared Systems Development Corp., Winter Park, FL) was liquid N₂ cooled. Its 0.1 mm 32 MCT detector elements with 0.112 mm pitch and cooled optical prefilter were designed by the manufacturer to closely match the spectral response of the video camera, so we used the same emissivity calibration as with the video camera.

The camera and the linear array viewed the sample through a 50:50 MWIR beam splitter coated on a 50 mm diameter ZnSe substrate 3 mm thick (Spectral Systems, Hopewell Junction, NY). The working distance from the objective to the sample was 60 mm. As shown in Fig. 1(b), the linear array was mounted on a laser table adjacent to the drop hammer, while the camera was mounted on the drop hammer itself. Mounting the camera on the drop hammer reduced image shaking since the sample and the camera experienced similar correlated vibrational histories. Image shaking was not a significant problem for the linear array since it already has lower spatial resolution and is looking at fast processes where there is not enough time for much shaking to occur. Both detectors were mounted on *xyz* translation stages to align the images and focus the objectives.

C. Image shaking

We characterized the image shaking by scratching a crosshair on a sapphire window and filming it during the assumed worst-case scenario, where the hammer kinetic energy was its maximum value of 225 J. Results are shown in Fig. 2 for three successive drops, where the impact occurred at about 10 ms after the trigger. In the 10 ms after impact, the image deflection was about 200 μ m. The maximum deflection of the sample was 1.15 mm at 50 ms. It is interesting that the deflection profile was reproducible from drop to drop within ~ 100 μ m. This makes the image shaking appear to be a deterministic rather than a random process, which suggests we might be able to strategically control and reduce the image shaking.

D. Noise floor for temperature determination

When a sapphire anvil is impacted by a striker, it produces triboluminescent emission¹⁸ that can interfere with pyrometric temperature measurements. Assuming that the temperature sensitivity is limited by the intensity of the triboluminescent

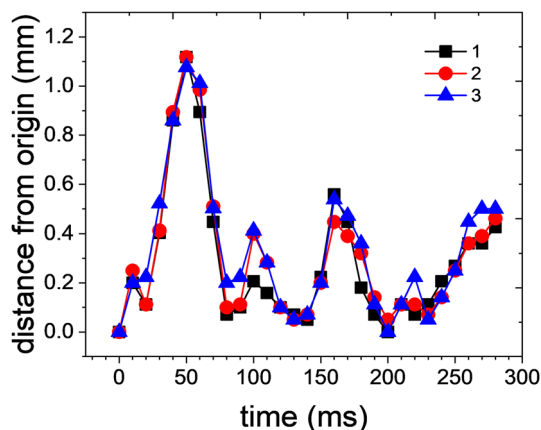


FIG. 2. Video image shaking with a 40'' drop with energy 225 J for three drops onto sapphire windows with an inscribed crosshair. During the fast explosion, which occurs at a time of a few milliseconds but lasts for just $\sim 200 \mu\text{s}$, the image shaking is $\sim 2 \mu\text{m}$.

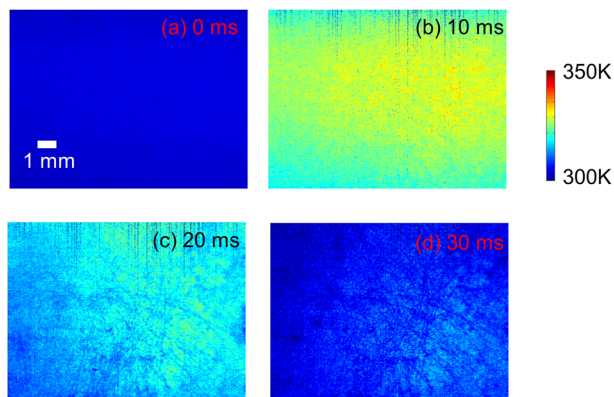


FIG. 3. Thermal images of a maximum-energy 225 J hammer drop onto a sapphire anvil without an energetic material used to determine the noise floor for MWIR temperature detection. The noise floor is set by the triboluminescent emission of the sapphire anvil impacted by the striker. At its peak, this spurious background emission has an apparent temperature rise from ambient temperature of about 30 K, so the noise floor is a few tens of K.

background from the sapphire window, we measured this background in control experiments with the results shown in Fig. 3, where the MWIR camera observed the pin striking the sapphire anvil directly with no intervening sample. As with the image deflection measurements, in Fig. 3, the hammer energy was at its maximum value of 225 J. The maximum MWIR emission from the sapphire anvil occurred shortly after the instant of impact near 10 ms. Although the sapphire emission is unlikely to be thermal emission, it can be converted to a characteristic single-color pyrometry temperature. At its peak, the sapphire background corresponds to a temperature of about 30 K above ambient. Thus, in the worst-case scenario, when the drop hammer energy was maximum and there was no sample to shield the anvil from the falling striker, the MWIR imaging system had a detection floor at an ambient temperature of about 30 K in temperature change.

III. SAMPLE PREPARATION

The explosive samples were crystals of RDX and HMX fully encased and suspended in a polymer binder, as depicted in

Fig. 1(d). The binder was Sylgard 182 (Dow Corning), a polydimethylsiloxane (PDMS) elastomer. RDX and HMX were dissolved in acetone and recrystallized once to assure purity. Crystals were grown in small beakers by slow evaporation over several days. The crystals were approximately 0.5 mm or 1 mm in the longest dimension. It is known that there is a crystal size dependence in drop-hammer experiments,¹⁹ but we have not yet performed size-dependent experiments. By visual inspection and polarized optical microscopy, the crystals appeared to be primarily single crystals with some much smaller crystallites clinging to the faces. The PDMS was mixed in a 10:1 weight ratio (base/accelerator) and degassed under vacuum. A 300 μm thick base layer of PDMS was deposited on the sapphire and allowed to cure at 100 °C for 15 min. After cooling to room temperature, a second PDMS layer 500 μm thick was spread over the base layer, and RDX or HMX crystals were immersed in the semi-liquid PDMS with tweezers. After curing at 100 °C for 15 min and cooling, a third 500 μm thick PDMS layer was spread over the crystal to make certain that it was fully encased by PDMS. The final assembly was cured at 100 °C for 60 min. Calorimetry and gravimetric analyses have shown no significant thermal decomposition for RDX or HMX for such brief exposures to temperatures even as high as 200 °C.¹⁶

IV. ULTRASONIC HAMMER

In the ultrasound initiation experiments, the RDX or HMX crystals were coated with a thin layer of lubricant [M_w 400 polyethylene glycol (PEG) from Sigma Aldrich] before being embedded in the PDMS polymer in the same manner as the drop hammer samples, so the drop and ultrasonic hammer samples differ only in the small quantity of lubricant between the explosive and the binder. The tip of a 20 kHz acoustic horn (CV-33, Sonics and Materials, Inc.) was pressed against the polymer encasement with a force of 10^6 N/m^2 .¹⁴⁻¹⁶ The tip oscillation amplitude was about 100 μm . As discussed in previous studies,^{15,16,20} in the absence of lubricant, the crystal and polymer tend to oscillate synchronously and there is minimal rubbing and weak heating. But with the lubricant, the crystal faces are free to rub against the surrounding polymer, which heats the crystal surface to explosion at a rate of roughly 10 000 K/s.¹⁵ We call the ultrasound heating method an “ultrasonic hammer”¹⁵ since the tip of the sonic horn hammers away at 20 kHz at the polymer-encased crystals.

V. RESULTS

Here we present representative results obtained from a smaller (0.5 mm) and a larger (1 mm) RDX crystal and a larger (1 mm) HMX crystal, initially at 300 K, using the maximum drop height of 40'' and the maximum drop energy of 225 J. Figure 4 shows before and after optical images of a polymer-encased HMX crystal of nominal size 1 mm. In Fig. 4(b), the recovered sample shows a depression with the outline of the striker pin in the PDMS encasement as well as carbonized material from the crystal explosion.

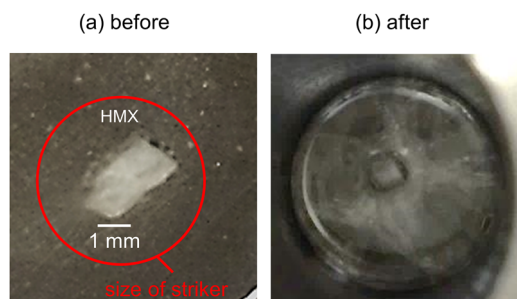


FIG. 4. Static optical microscope images of a polymer-encased HMX crystal for drop-hammer testing (a) before impact and (b) after impact, showing the impact crater left by the 0.5" striker in the polymer along with explosive residue.

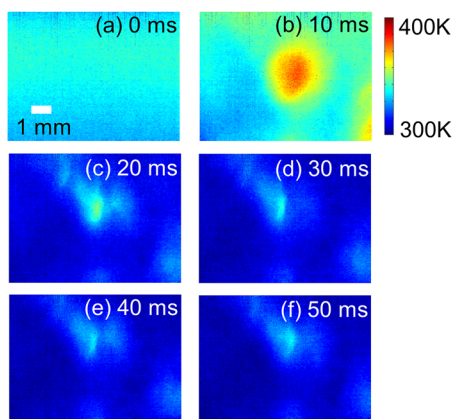


FIG. 5. Selected video images at 10 ms intervals from a 40'' impact with a polymer-encased 0.5 mm RDX crystal.

MWIR video images for the 0.5 mm polymer-encased RDX crystal with a 225 J drop from 40'' are shown in Figs. 5 and 6, where time = 0 denotes a time that precedes the impact by a few milliseconds. In Fig. 5, the MWIR images were acquired with the video camera at 10 ms intervals. The crystal temperature peaked at 10 ms, where it appeared to be about 400 K. However, the 10 ms interframe time is too short to time resolve the actual crystal explosion, so the image Fig. 5(b) does not represent the actual peak temperature; rather it represents the single-color pyrometry effective temperature of the explosion derived from the MWIR intensity averaged over the 10 ms camera acquisition window.¹⁴ Figure 5 also shows that

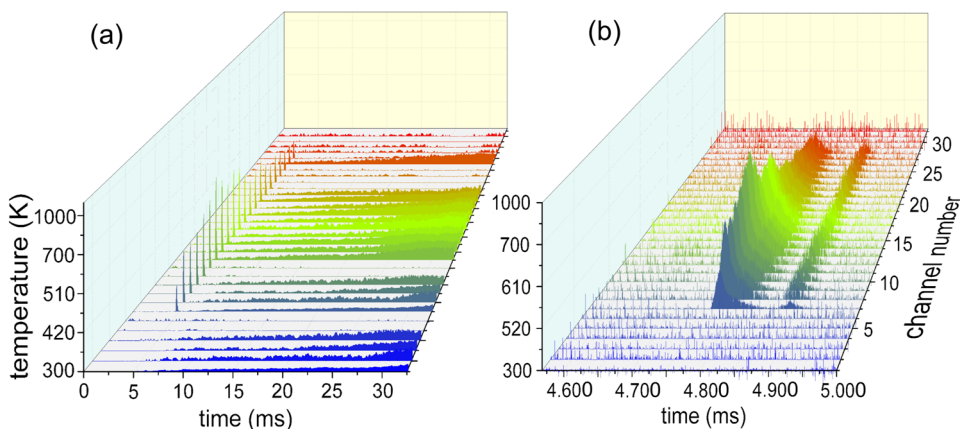


FIG. 6. Output of the linear MWIR array during a 40'' drop impact with the polymer-encased 0.5 mm RDX crystal, obtained simultaneously with the video images in Fig. 5. The linear array is measuring the temperature in a strip 0.5 mm wide running through the middle of the crystal. (a) The full 32 ms record shows an instantaneous fast explosion at about 5 ms and a much slower burning lasting many tens of milliseconds. (b) The same record on an expanded scale showing the two-part explosion.

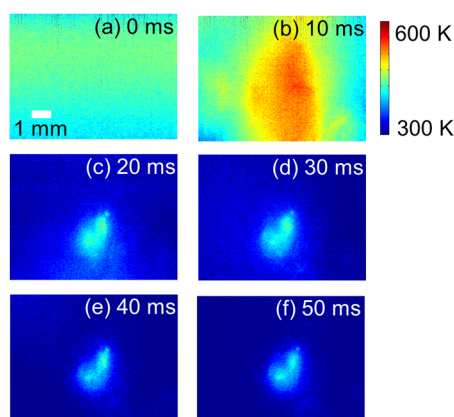


FIG. 7. Selected video images at 10 ms intervals from a 40'' impact with a polymer-encased 1 mm RDX crystal.

the sample stays warm for many tens of milliseconds after the explosion.

Figure 6 shows line-out images from the smaller 0.5 mm RDX crystal acquired simultaneously with the video in Fig. 5, using the much faster linear array detector. Figure 6(a) shows an apparently instantaneous temperature burst to about 1000 K peak occurring at about 4.8 ms, followed by a much slower, lower-temperature burn. An expanded time version of the linear array output in Fig. 6(b) shows that the RDX crystal explosion lasted approximately 150 μ s, and the main explosion was followed by a second, weaker explosion about 100 μ s later.

Figures 7 and 8 show the same type of measurement on a larger 1 mm polymer-encased RDX crystal, again with a 225 J drop from 40''. This larger crystal has about ten times the volume of the crystal used for Figs. 5 and 6, and the explosion was much more violent. As shown in Fig. 7(b), the camera recorded a peak temperature of about 600 K, and again the sample stayed warm for many tens of milliseconds. The linear array data in Fig. 8(a) show that the explosion temperature peak was actually about 1500 K. Figure 8(b) shows that the RDX explosion occurred in two stages, but the second stage appeared sooner and was hotter than with the smaller RDX crystal.

Figures 9 and 10 show results from a polymer-encased 1 mm HMX crystal with a 225 J drop from 40'' (1.02 m). The video camera results in Fig. 9 show an explosion at 10 ms

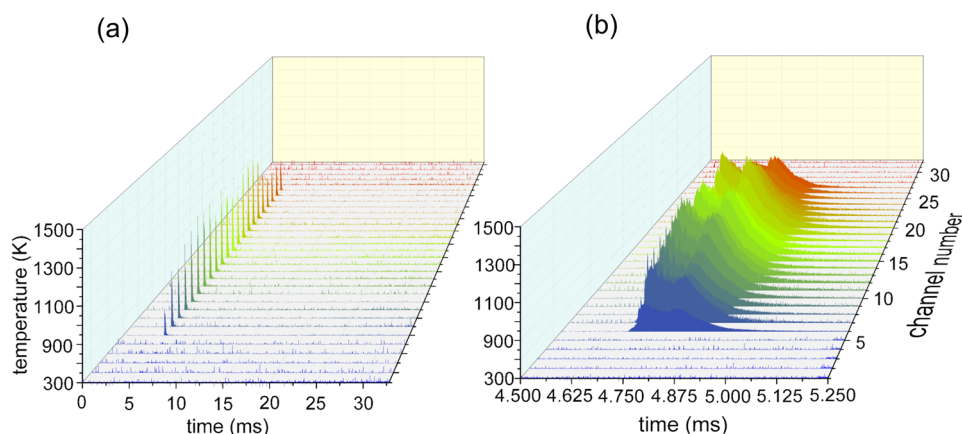


FIG. 8. Output of the linear MWIR array with a 40° impact with the polymer-encased 1 mm RDX crystal. (a) The full 32 ms record. (b) The same record on an expanded scale showing the two-part explosion.

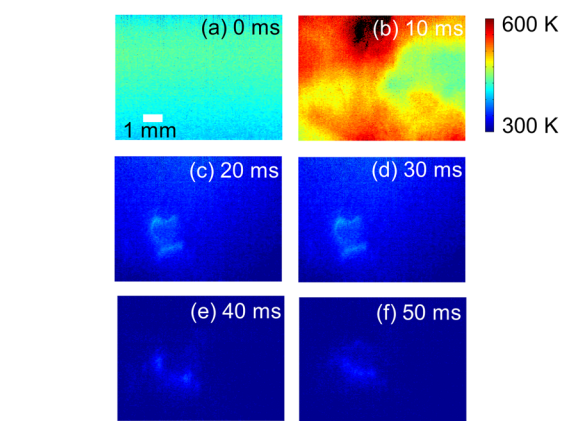


FIG. 9. Selected MWIR video images at 10 ms intervals from a 40° impact with a polymer-encased 1 mm HMX crystal.

[Fig. 9(b)] which was much more violent and widespread than with RDX, which is consistent with HMX being the higher-performance explosive. There was not much warm material remaining after the big explosion, which suggests that the HMX explosion completely consumed the energetic material. The linear array results in Fig. 10 show an intense 2-stage explosion starting at about 5.3 ms and reaching a peak temperature of about 3000 K. Figure 10(b) shows that the second stage of the HMX explosion was hotter than the first, unlike the RDX explosions.

Figures 11(a) and 11(c) compare time-dependent temperature profiles for drop-hammer experiments on RDX and

HMX. These profiles are the time-dependent temperature average within a strip 0.3 mm wide running through the hottest part of the crystal explosions shown in Figs. 6(b), 8(b), and 10(b), and each displayed temperature is the average over a 5 μ s time window.¹⁴ Each time axis in the panels of Fig. 11 has an arbitrary time shift accounting for variable dead times, to put the explosion in the center of the panel. The time shift was about 5 ms for the drop hammer and a few tens of milliseconds for the ultrasound.

The temperature rise times (the approximate time interval between the 10% and 90% of the temperature peak) in Figs. 11(a) and 11(b) were quite a bit slower than the instrument time resolution of 1 μ s, so the linear array has accurately determined these rise times. With the smaller RDX crystal [Fig. 11(a)], the first explosion had a rise time of 10 μ s and the second and much lower temperature explosion was about 150 μ s after the first. With the larger RDX crystal [Fig. 11(a)], the first explosion was much hotter than with the smaller crystal, and it had a rise time of 15 μ s. The second explosion was about 90 μ s after the first.

With the HMX crystal, Fig. 11(b) shows that there was also a two-phase explosion. Both phases had rise times of about 10 μ s. The second, more intense explosion was about 90 μ s after the first.

In Figs. 11–13, we compare the drop hammer initiation of RDX and HMX crystals to the initiation of similarly sized RDX and HMX crystals using high-speed (20 kHz) frictional rubbing produced by using the ultrasonic hammer. Figures 12 and 13 show the linear array output during the explosion

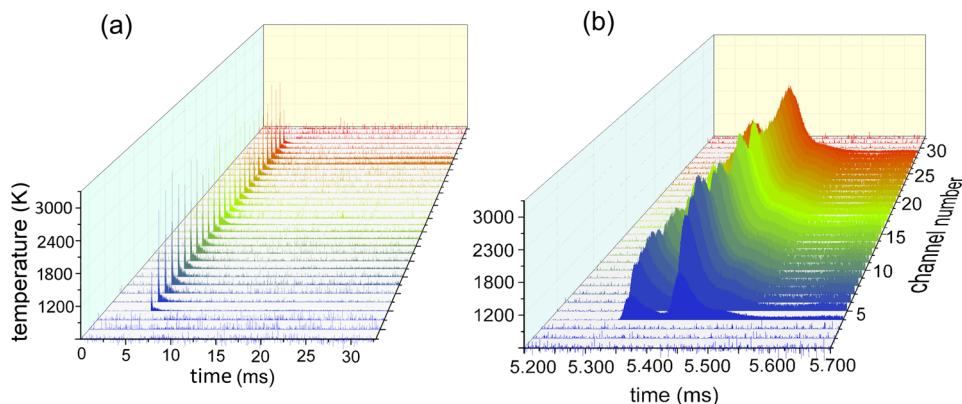


FIG. 10. Output of the linear MWIR array during a 40° impact with a polymer-encased 1 mm HMX crystal. (a) The full 32 ms record. (b) The same record on an expanded scale showing the two-part explosion.

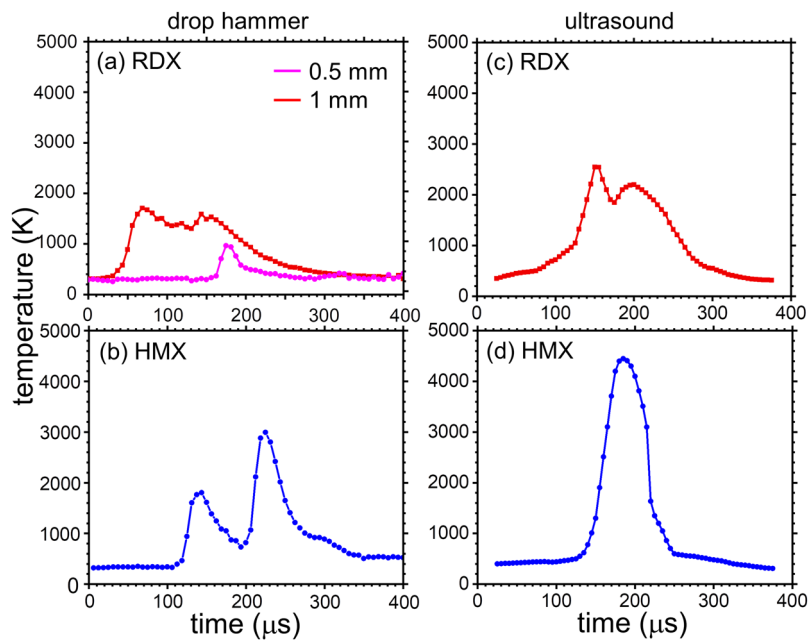


FIG. 11. Comparison of time-dependent temperature profiles for polymer-encased RDX and HMX crystals with a 40'' drop with crystals initiated by fast rubbing with an ultrasonic hammer. These are the temperatures from a 0.5 mm wide strip at the center of the crystals. (a) Smaller 0.5 mm and larger 1 mm RDX crystals with a drop hammer. (b) A 1 mm HMX crystal with a drop hammer. (c) A 1 mm RDX crystal with an ultrasonic hammer. (d) A 1 mm HMX crystal with an ultrasonic hammer. All the panels have an arbitrary time shift to locate the fast explosion in the center of the panel. This shift is about 5 ms for the drop hammer and a few tens of milliseconds for the ultrasonic hammer.

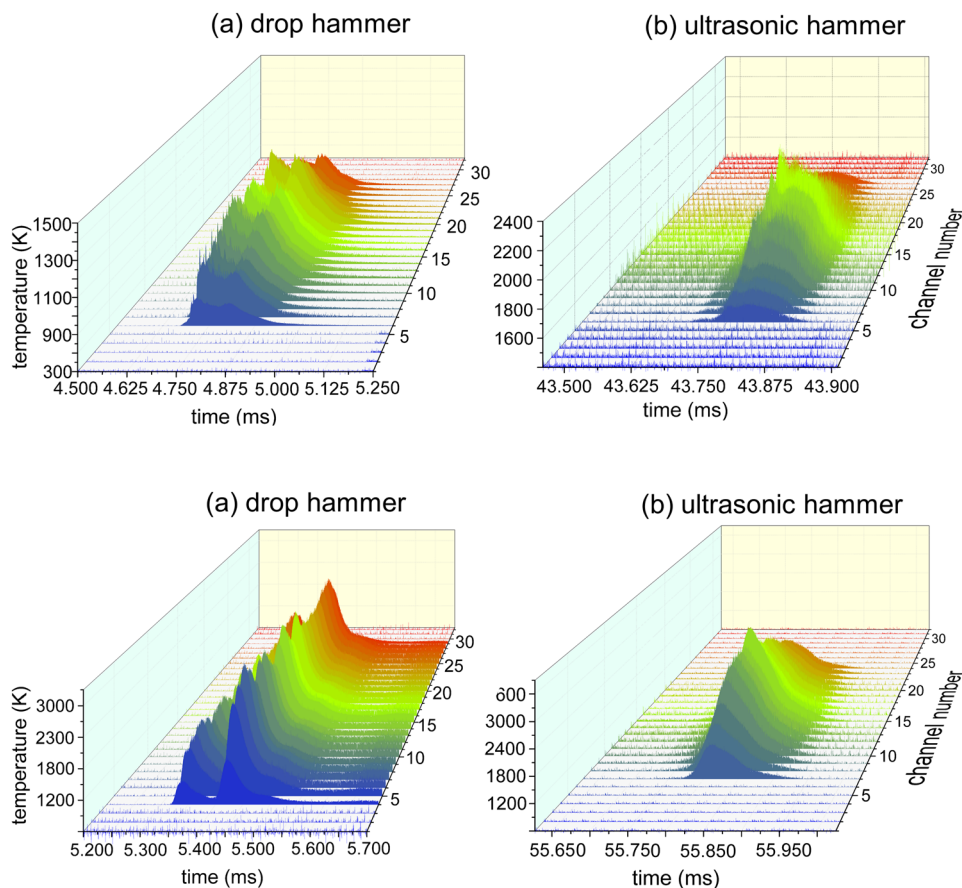


FIG. 12. Comparison of thermal profiles for a 1 mm RDX crystal (a) with a 40'' drop from the drop hammer or (b) initiation using the ultrasonic hammer.

FIG. 13. Comparison of thermal profiles for a 1 mm HMX crystal (a) with a 40'' drop from the drop hammer or (b) initiation using the ultrasonic hammer.

phase for the larger RDX and HMX crystals, respectively. With ultrasound initiation, the rise times are considerably slower than with the drop hammer, 40-60 μs compared to the 10-20 μs obtained with the drop hammer. The peak temperatures, however, are considerably higher with ultrasound. With both ultrasound and drop hammer initiation, RDX has a two-part explosion. With the drop hammer, HMX had a

two-part explosion, but with ultrasound, HMX had a single-part explosion.

VI. DISCUSSION

We have described a drop hammer that uses dual MWIR detectors that, when operating simultaneously, have the

capability of measuring, with high time and space resolution, the time-dependent temperatures of both the fast explosion and the subsequent slower combustion of materials not consumed during the explosion.

Two factors that limit the accuracy of high-speed thermal imaging measurements on impacted materials are image shaking and the spurious MWIR light produced by the drop-hammer components themselves. We greatly reduced shaking by mounting the video camera directly on the drop hammer [Figs. 1(a) and 1(b)], and in this configuration, the shaking, at its present level, has no effect on our ability to measure the fast explosion with high spatial resolution. The fast explosion occurs a few milliseconds after trigger, and according to Figs. 11–13, it typically lasts 200–300 μs . Figure 2 shows that the camera image shakes about 0.2 mm during the first 15 ms, so this shaking movement has an apparent velocity of about 0.01 m/s. Thus during the brief explosion which lasts $\sim 200 \mu\text{s}$, the total shaking amplitude is $\sim 2 \mu\text{m}$. The shaking during the actual explosion is therefore negligible compared to the diffraction-limited MWIR resolution of 15 μm .

Our single-color pyrometer interprets total MWIR intensity in the 3.7–4.8 μm wavelength range as representing a temperature T , so any spurious MWIR emission from impacted components of the drop hammer creates a noise floor for our temperature determination. The vast majority of spurious MWIR emission originates from the impact of the striker with the sapphire anvil, which causes the sapphire to produce a brief burst of triboluminescence lasting about 100 ns.¹⁸ According to Fig. 3, when the spurious emission was at its maximum, the corresponding effective pyrometric temperature T was about 30 K. We emphasize that this is a worst-case scenario since this noise floor corresponds to the maximum-energy impact, and during experiments, it is quite likely that the sample located between the striker and the sapphire anvil will take up some of the energy input to the anvil. Thus our thermal-imaging drop hammer should be capable of resolving impact-induced temperature increases of even a few tens of K above ambient.

The thermal profiles for impact-initiated RDX and HMX all have a two-part fast explosion. With the smaller RDX crystal, the interval between the two parts was about 150 μs , and with the larger RDX or HMX crystals, this interval was 90 μs . This raises the question as to whether the two-part explosion is a consequence of the experimental design or an intrinsic process due to thermomechanical kinetics of the explosives. If the former, it would most likely be due to the way the striker bounces⁴ when it impacts the sample. The bouncing causes the loading of the sample to have an oscillatory component after the initial compression.⁴ The striker velocity in our experiments was about 10 m/s, and the size of the explosive targets was on the order of 0.5–1.0 mm. In the roughly 100 μs interval between explosions, the striker could move about 1 mm, which is comparable to the sample dimensions, so this argument cannot rule out the possibility that the two-part explosions result from the way the striker bounces off the target. However the time interval between explosions, 150 μs , was quite different for the smaller RDX crystal than for the larger RDX and HMX crystals, where it was 90 μs . Williamson and co-workers¹⁰ detected similar two-part emission bursts from HMX powder

in a drop hammer with about one-half the impact velocity used here. The fact that this time interval was similar with two quite different drop hammer instruments and that the time intervals were significantly different in our apparatus using different sample materials suggests that the two-part explosion is indeed a property of the impacted explosive.

On comparing the drop hammer to a quite different initiation method, the ultrasonic hammer, the fast explosion temperature profiles in Fig. 11 had similar durations of 100–200 μs . However the temperature rise time was quite a bit faster with the drop hammer and the peak temperatures were quite a bit greater with ultrasound. This admittedly small set of results seems to show that the two initiation methods result in quite different explosion processes. When the impactor arrives, it creates widespread plastic deformation, cracking, and hot-spot generation throughout the crystal, whereas the ultrasonic hammer inputs heat to the faces of the crystal (the crystal-polymer interface) by high-speed frictional rubbing. Based on these considerations, we attribute the faster rise times created by the drop hammer to the presence of initiation sites spread widely throughout the crystal interior, whereas the ultrasonic hammer produces hotter initiation sites only on the crystal surface. In order to produce a crystal explosion with ultrasound, the reaction has to take time to propagate from the crystal surfaces to the crystal interior. The higher temperatures associated with ultrasound compared to drop hammer low-velocity impact seem likely to result from ultrasound inputting more heat and that heat is localized at the crystal surfaces.

VII. CONCLUSIONS

The drop hammer with two simultaneous thermal imagers can measure the temperature evolution of explosives with time and space resolution sufficient to observe both the fast initial explosion and the slower combustion of material not consumed during the explosion. RDX initiation and HMX initiation by using the drop hammer and ultrasonic hammer have different mechanisms which result in drop-hammer initiated explosions with faster rise times and lower temperatures than the ultrasonic hammer.

ACKNOWLEDGMENTS

The research described in this study was based on the work supported by the U.S. Air Force Office of Scientific Research under No. FA9550-16-1-0042. Zhiwei Men acknowledges support from the Office of China Postdoctoral Council for work performed at the University of Illinois.

¹L. R. Simpson and M. F. Foltz, Report No. UCRL-ID-119665, 1995.

²S. N. Heavens and J. E. Field, *Proc. R. Soc. A* **338**(1612), 77 (1974).

³J. E. Field, S. M. Walley, W. G. Proud, H. T. Goldrein, and C. R. Siviour, *Int. J. Impact Eng.* **30**(7), 725 (2004).

⁴C. S. Coffey and V. F. De Vost, *Propellants, Explos., Pyrotech.* **20**(3), 105 (1995).

⁵G. Zhang and B. L. Weeks, *Propellants, Explos., Pyrotech.* **35**(5), 440 (2010).

⁶J. E. Field, G. M. Swallowe, and S. N. Heavens, *Proc. R. Soc. A* **382**(1782), 231 (1982).

⁷W. J. Dixon and A. M. Mood, *J. Am. Stat. Assoc.* **43**(241), 109 (1948).

- ⁸R. H. B. Bouma, A. G. Boluijt, H. J. Verbeek, and A. E. D. M. van der Heijden, *J. Appl. Phys.* **103**(9), 093517 (2008).
- ⁹J. J. Phillips, *Propellants, Explos., Pyrotech.* **37**(2), 223 (2012).
- ¹⁰D. M. Williamson, S. Gymer, N. E. Taylor, S. M. Walley, A. P. Jardine, A. Glauser, S. French, and S. Wortley, *RSC Adv.* **6**(33), 27896 (2016).
- ¹¹S. M. Walley, J. E. Field, R. A. Biers, W. G. Proud, D. M. Williamson, and A. P. Jardine, *Propellants, Explos., Pyrotech.* **40**(3), 351 (2015).
- ¹²D. L. Woody, *J. Appl. Phys.* **72**, 783 (1992).
- ¹³D. L. Woody, *Rev. Sci. Instrum.* **63**(3), 2030 (1992).
- ¹⁴Z. Men, K. S. Suslick, and D. D. Dlott, *J. Phys. Chem. C* **122**(26), 14289 (2018).
- ¹⁵S. You, M.-W. Chen, D. D. Dlott, and K. S. Suslick, *Nat. Commun.* **6**, 6581 (2014).
- ¹⁶M.-W. Chen, S. You, K. S. Suslick, and D. D. Dlott, *Rev. Sci. Instrum.* **85**(2), 023705 (2014).
- ¹⁷M.-W. Chen, S. You, K. S. Suslick, and D. D. Dlott, *Appl. Phys. Lett.* **104**(6), 061907 (2014).
- ¹⁸J. Wang, W. P. Bassett, and D. D. Dlott, *J. Appl. Phys.* **121**(8), 085902 (2017).
- ¹⁹R. W. Armstrong, S. G. Bardenhagen, and W. L. Elban, *Int. J. Energ. Mater. Chem. Propul.* **11**, 413 (2012).
- ²⁰Z. A. Roberts, A. D. Casey, I. E. Gunduz, J. F. Rhoads, and S. F. Son, *J. Appl. Phys.* **122**(24), 244901 (2017).